Comparison of the Manganese Oxygen-Evolving Complex in Photosystem II of Spinach and *Synechococcus* sp. with Multinuclear Manganese Model Compounds by X-ray Absorption Spectroscopy

Victoria J. DeRose,[‖,†] Ishita Mukerji,[‖,‡] Matthew J. Latimer,[‖] Vittal K. Yachandra,[*,§] Kenneth Sauer,[*,‖,§] and Melvin P. Klein[*,§]

Contribution from the Department of Chemistry, University of California—Berkeley, and Structural Biology Division, Lawrence Berkeley Laboratory, Berkeley, California 94720

Received December 3, 1993[⊗]

Abstract: The evaluation of Mn X-ray absorption fine structure (EXAFS) studies on the oxygen-evolving complex (OEC) from photosystem II is described for preparations from both spinach and the cyanobacterium *Synechococcus* sp. poised in the S_1 and S_2 states. In addition to reproducing previous results suggesting the presence of bis(μ-oxo)-bridged Mn centers in the OEC, a Fourier transform peak due to scatterers at an average distance of >3 Å is detected in both types of preparation. In addition, subtle but reproducible changes are found in the relative amplitudes of the Fourier transform peaks due to mainly O (~1.8 Å) and Mn (~2.7 Å) neighbors upon cryogenic advance from the S_1 to the S_2 state. Analysis of the peak due to scatterers at ~3 Å favors assignment to (per 4 Mn in the OEC) 1–2 heavy atom (Mn, Ca) scatterers at an average distance of 3.3–3.4 Å. The EXAFS data of several multinuclear Mn model compounds containing such scattering interactions are analyzed and compared with the data for the OEC. Structural models for the OEC are evaluated on the basis of these results.

Introduction

The photosynthetic energy transduction path in plants, algae, and cyanobacteria acquires the reducing equivalents necessary for CO_2 fixation by using light energy to abstract 4 electrons from water. Reaction 1 is catalyzed, in conjunction with electron-

$$2H_2O \rightarrow 4e^- + O_2 + 4H^+ \quad (1)$$

transfer components from the photosystem II reaction center, by a complex of 4 Mn atoms known as the oxygen evolving complex (OEC).[1] Both chloride and calcium ions have also been implicated as cofactors in the reaction. Water oxidation in photosystem II (PSII) is a stepwise process wherein each of 4 sequential photons absorbed by the reaction center powers the advance of the oxygen-evolving complex through the S-state intermediates S_0–S_4. Upon reaching the S_4 state, the complex releases O_2 and returns to S_0. In the dark, the complex "relaxes" to a predominantly S_1 population, and from this state the OEC can be trapped in S_2 by a low-temperature illumination protocol. The PSII reaction center components are thought to be similar to the crystallographically characterized reaction center from non-oxygen-evolving bacterial photosystems. The structure of the multinuclear Mn complex, however, is unknown and the subject of active investigation.

We and others have studied the structure of Mn in the OEC using the technique of X-ray absorption fine structure (EXAFS)[2] spectroscopy. These studies measure the average radial distribution function of scatterers around the Mn atoms, allowing estimates of the distances, numbers, and types of atoms near the Mn.[3] An earlier series of papers from this group reported Mn–metal interactions at 2.7 Å and Mn–O interactions at 1.75 Å,[4a] and an additional highly disordered shell of light atom (O, N) scatterers at ~2 Å.[4] The results of X-ray absorption edge studies indicated an oxidation of Mn upon advance to S_2,[4a,c,5] and comparison of the edge structure with model compounds is suggestive of Mn in the oxidation states $Mn^{III}_2Mn^{IV}_2$ in the S_1 state.[4c] Similar results were found for both PSII-enriched membrane preparations from spinach chloroplasts and for detergent-solubilized OEC preparations from the thermophilic cyanobacterium *Synechococcus* sp.[4b] From these results on samples poised in both the S_1 and S_2 states, it was predicted that the OEC contains binuclear bis(μ-oxo)-bridged Mn units whose structures remain largely unchanged upon the oxidation of a Mn(III) to a Mn(IV) in the advance to S_2.[1c]

* To whom correspondence should be addressed.
‖ Department of Chemistry, University of California—Berkeley.
§ Structural Biology Division, Lawrence Berkeley Laboratory.
† Present address: Department of Chemistry, Northwestern University, Evanston, IL 60208.
‡ Present address: Department of Chemistry, Princeton University, Princeton, NJ 08544.

⊗ Abstract published in *Advance ACS Abstracts,* May 1, 1994.

(1) For recent reviews of the OEC, see: (a) Debus, R. J. *Biochim. Biophys. Acta* **1992**, *1102*, 269–352. (b) Hansson, Ö.; Wydrzynski, T. *Photosynth. Res.* **1990**, *23*, 131–162. (c) Sauer, K.; Yachandra, V. K.; Britt, R. D.; Klein, M. P. In *Manganese Redox Enzymes*; Pecoraro, V. L., Ed.; VCH Publishers: New York, 1992; pp 141–175.

(2) Abbreviations used: bipy, 2,2′-bipyridine; Chl, chlorophyll; dbm, dibenzoylmethane; DCBQ, 2,6-dichloro-*p*-benzoquinone; DMSO, dimethyl sulfoxide; EDTA, ethylenediaminetetraacetic acid; EPR, electron paramagnetic resonance; EXAFS, extended X-ray absorption fine structure; HIm, imidazole; MES, 4-morpholineethanesulfonic acid; OAc, acetato (O_2CCH_3); PMSF, (phenylmethyl)sulfonyl fluoride; tacn, 1,4,7-triazacyclononane; XAS, X-ray absorption spectroscopy.

(3) For reviews of EXAFS, see: (a) Powers, L. *Biochim. Biophys. Acta* **1982**, *683*, 1–38. (b) Scott, R. A. *Methods Enzymol.* **1985**, *117*, 414–459. (c) Cramer, S. P. In *X-ray Absorption: Principles, Applications, and Techniques of EXAFS, SEXAFS, and XANES*; Koningsberger, D. C., Prins, R., Eds.; Wiley-Interscience: New York, 1988; pp 257–320. (d) Lee, P. A.; Citrin, P. H.; Eisenberger, P.; Kincaid, B. M. *Rev. Mod. Phys.* **1981**, *53*, 769–806.

(4) (a) Yachandra, V. K.; Guiles, R. D.; McDermott, A. E.; Cole, J. L.; Britt, R. D.; Dexheimer, S. L.; Sauer, K.; Klein, M. P. *Biochemistry* **1987**, *26*, 5974–5981. (b) McDermott, A. E.; Yachandra, V. K.; Guiles, R. D.; Cole, J. L.; Dexheimer, S. L.; Britt, R. D.; Sauer, K.; Klein, M. P. *Biochemistry* **1988**, *27*, 4021–4031. (c) Guiles, R. D.; Yachandra, V. K.; McDermott, A. E.; Cole, J. L.; Dexheimer, S. L.; Britt, R. D.; Sauer, K.; Klein, M. P. *Biochemistry* **1990**, *29*, 486–496. (d) Guiles, R. D.; Zimmermann, J.-L.; McDermott, A. E.; Yachandra, V. K.; Cole, J. L.; Dexheimer, S. L.; Britt, R. D.; Wieghardt, K.; Bossek, U.; Sauer, K.; Klein, M. P. *Biochemistry* **1990**, *29*, 471–485. (e) Yachandra, V. K.; DeRose, V. J.; Latimer, M. J.; Mukerji, I.; Sauer, K.; Klein, M. P. *Science* **1993**, *260*, 675–679.

(5) Ono, T.; Noguchi, T.; Inoue, Y.; Kusunoki, M.; Matsushita, T.; Oyanagi, H. *Science* **1992**, *258*, 1335–1337.

0002-7863/94/1516-5239$04.50/0

Most Mn model compounds of nuclearity >2 contain Mn–Mn distances at >3 Å.[6] In EXAFS studies, the detection and analysis of metal scatterers at distances greater than 3 Å can be difficult due to the combined effects of enhanced disorder, interference from other ligands, and the $1/R^2$ dependence on scattering amplitude.[7] Evidence for such an interaction was not consistently reported in the above EXAFS studies,[4d] leading to a prediction that the binuclear Mn units in the OEC were separated by >3 Å.[1c] More recent EXAFS studies of Mn in the OEC, at substantially lower sample temperatures and with improved signal to noise ratio, have provided evidence for scatterers at >3 Å in addition to the interaction at 2.7 Å.[8] These experiments include various combinations of oxygen-evolving preparations and EXAFS analysis techniques, and while the presence of a Mn–Mn distance of 2.7 Å is generally agreed upon, both the characteristics of the bridging and terminal ligand distances and the analysis of the longer distance have differed between the reporting groups. For example, George et al.[8a] report Mn scatterers at a distance of 3.3 Å in angle-dependent EXAFS studies of oriented whole spinach chloroplasts. It was found that the scatterers at this distance exhibited significant dichroism. In their analysis, however, the short ~1.8-Å bridging interaction was not detected; rather, an average distance of 1.9 Å was found for the first shell of light atoms. Penner-Hahn et al.[8b] also reported at least one and possibly two shells of scatterers at >3 Å in EXAFS experiments using more refined "core" preparations from spinach, but again the 1.8-Å interaction did not dominate the first shell of scatterers. In a third study that included a different detergent-solubilized OEC preparation from spinach, MacLachlan et al.[8c] reproduced the 1.8-Å shell along with the 2.7-Å scatterers but differed from the above experiments by predicting a shell of Ca at a significantly longer distance of 3.7 Å. These results all have different implications for a structural model of the OEC.

In this paper we report low-temperature EXAFS measurements and analysis of membrane PSII preparations from spinach and of PSII particles from *Synechococcus* sp. with significant improvement in signal to noise ratio over our previous studies. The results are compared with the EXAFS of several multinuclear Mn model compounds. The results presented here both confirm the existence of scatterers at >3 Å and reaffirm the dominance of short bridging atoms at 1.8 Å in both of these OEC preparations. The analysis by EXAFS of longer (>3 Å) Mn–Mn scatterer interactions is investigated for multinuclear Mn model compounds and the OEC. Finally, various structural models for the OEC are analyzed with respect to the parameters derived from these EXAFS studies.

Methods

PSII Oxygen-Evolving Preparations from Spinach and *Synechococcus* sp. Oxygen-evolving particles from *Synechococcus* sp. were prepared as previously described[4b,9] with specific activities of 3000–4000 (μmol of O_2/mg of Chl)/h. Detergent-extracted PSII particles were pelleted by centrifugation at 4 °C, 300000*g*, for 3–4 h. The pellet was resuspended in sucrose buffer (50 mM MES, pH 6.5, 5 mM $CaCl_2$, 400 mM sucrose, 200 μM PMSF), centrifuged as before, resuspended in the same buffer minus sucrose, and centrifuged again for 4–8 h. The resulting pellet was mixed thoroughly with approximately one-third volume of glycerol, and the mixture was packed tightly into hollow Lucite sample holders backed with Mylar tape, of approximately 0.12-mL volume. The final Chl concentration in the EXAFS holders was ~10 mg/mL; assuming 60–75 Chl/PSII,[4b] this was 700–800 μM Mn concentration.

PSII-enriched membranes were isolated from spinach using a slightly modified "BBY preparation"[10] with final activities of ~600 (μmol of O_2/mg of Chl)/h. The membranes were resuspended in buffer (50 mM MES pH 6, 400 mM sucrose, 5 mM $CaCl_2$) and pelleted by centrifugation at 4 °C, 39000*g*, for 1 h. The pellets were then loaded directly into the Lucite sample holders. The final Mn concentration in these samples was ~600–750 μM Mn, assuming 30 mg of Chl/mL and 200–250 Chl/PSII.

For both types of samples, EDTA or other divalent cation chelators were excluded from the preparations, because these suppress the EPR-detectable six-line spectrum from Mn^{2+}, which is a useful monitor of sample degradation. Samples were loaded into holders under dim green light and dark-adapted for at least 1 h before being frozen in liquid nitrogen until use.

Oxygen evolution activity measurements were performed with a Clark-type oxygen electrode (Yellow Springs Instruments) with DCBQ (Sigma) as an electron acceptor. DCBQ was added from a stock solution in DMSO to a final concentration of 2 μM. Chlorophyll assays were performed on acetone extracts using the method of Arnon.[11] Chlorophyll concentrations used for oxygen evolution assays were ~10 μg/mL for *Synechococcus* PSII preparations and ~50 μg/mL for PSII membranes from spinach.

X-Band EPR spectroscopy with a Varian E-109 spectrometer, standard TE_{102} cavity, and Air Products liquid-helium cryostat was performed directly on the samples in their XAS holders before and after exposure to X-rays. Samples were monitored for EPR-detectable Mn^{2+} and for formation of the $g = 2$ multiline signal in the S_2 state. To poise them in the S_2 state, samples were cooled to 195 K and illuminated 5–10 min with a 400-W tungsten lamp thermally isolated from the sample by a 5-cm filter containing 5% aqueous $CuSO_4$. The intensity of the multiline signal was found to be degraded by ≤10% following exposure to X-rays.

The following multinuclear Mn model complexes were generously provided by our collaborators: $[Mn^{III}_2O(OAc)_2(tacn)_2]^{2+}$ (**1**);[12] $[Mn^{III}_3O(C_6H_5CO_2)_6(ImH)_3]^+$ (**2**);[13] $Mn^{IV}_3O_4Cl_2(bipy)_4]^{2+}$ (**3**);[14] $[Mn^{III}_4O_2(OAc)_7(bipy)_2]^+$ (**4**);[15] $[Mn^{III}_3Mn^{IV}O_3Cl(OAc)_3(dbm)_3]$ (**5**).[16] XAS samples were made and data obtained as previously described.[4d] XAS data for **4** were obtained at a sample temperature of 180 K; data for all other models were taken at a sample temperature of 10 K.

X-ray Absorption Spectroscopy. XAS data were collected on beamlines X19A and X9A at the National Synchrotron Light Source (NSLS) at Brookhaven National Laboratory using Si[111] (X19A) and Si[220] (X9A) monochromators.

Sample temperature was maintained at 10 K with a liquid-helium cryostat (Oxford Systems, Oxford, England). Data were collected using fluorescence detection at a right angle to the incoming beam, with a 13-element Ge solid-state X-ray fluorescence detector (Canberra Instruments; generous loans from

(6) (a) Wieghardt, K. *Angew. Chem., Int. Ed. Engl.* **1989**, *28*, 1153–1172. (b) Pecoraro, V. L. *Photochem. Photobiol.* **1988**, *48*, 249–264. (c) Christou, G. *Acc. Chem. Res.* **1989**, *22*, 328–335. (d) Armstrong, W. H. In *Manganese Redox Enzymes*; Pecoraro, V. L., Ed.; VCH: New York, 1992; pp 261–286.

(7) Scott, R. A.; Eidsness, M. K. *Comments Inorg. Chem.* **1988**, *7*, 235–267.

(8) (a) George, G. N.; Prince, R. C.; Cramer, S. P. *Science* **1989**, *243*, 789–791. (b) Penner-Hahn, J. E.; Fronko, R. M.; Pecoraro, V. L.; Yocum, C. F.; Betts, S. D.; Bowlby, N. R. *J. Am. Chem. Soc.* **1990**, *112*, 2549–2557. (c) MacLachlan, D. J.; Hallahan, B. J.; Ruffle, S. V.; Nugent, J. H. A.; Evans, M. C. W.; Strange, R. W.; Hasnain, S. S. *Biochem. J.* **1992**, *285*, 569–576.

(9) DeRose, V. J.; Yachandra, V. K.; McDermott, A. E.; Britt, R. D.; Sauer, K.; Klein, M. P. *Biochemistry* **1991**, *30*, 1335–1341.

(10) Berthold, D. A.; Babcock, G. T.; Yocum, C. F. *FEBS Lett.* **1981**, *134*, 231–234.

(11) Arnon, D. *Plant Physiol.* **1949**, *24*, 1–15.

(12) Wieghardt, K.; Bossek, U.; Ventur, D.; Weiss, J. *J. Chem. Soc., Chem. Commun.* **1985**, 347–349.

(13) (a) Vincent, J. B.; Chang, H.-R.; Folting, K.; Huffman, J. C.; Christou, G.; Hendrickson, D. N. *J. Am. Chem. Soc.* **1987**, *109*, 5703–5711. (b) Christou, G.; Vincent, J. B. In *Metal Clusters in Proteins*; Que, L., Ed.; ACS Symposium Series 372; American Chemical Society: Washington, DC, 1988; pp 238–255.

(14) Auger, N.; Girerd, J.-J.; Corbella, M.; Gleizes, A.; Zimmermann, J.-L. *J. Am. Chem. Soc.* **1990**, *112*, 448–450.

(15) Vincent, J. B.; Christmas, C.; Huffman, J. C.; Christou, G.; Chang, H.-R.; Hendrickson, D. N. *J. Chem. Soc., Chem. Commun.* **1987**, 236–238.

(16) Wang, S.; Folting, K.; Streib, W. E.; Schmitt, E. A.; McCusker, J. K.; Hendrickson, D. N.; Christou, G. *Angew. Chem., Int. Ed. Engl.* **1991**, *30*, 305–306.

Dr. S. Cramer and Dr. B. Chance).[17] Data were ratioed by the incoming intensity, measured with a scintillator photomultiplier as scatter from a piece of Kapton placed before the sample. Energy calibration was maintained by simultaneously measuring the X-ray absorption spectrum of $KMnO_4$.

XAS Data Analysis. EXAFS data were prepared for curve-fitting analysis using the program EXAFS.[4a,18] Each data set consisted of the sum of 10–20 scans (13 data channels per scan). It was found for many cases that weighting the data from the individual channels by a factor of $F/(T^{1/2})$, where F = counts due to Mn fluorescence (counts at energies above the absorption edge minus counts below) and T = total counts (including both Mn fluorescence and scatter), increased the signal to noise ratio in the added data. A linear fit to points before the absorption edge was subtracted, and data were normalized to an absorption amplitude of unity at the edge by extrapolation of a second-order polynomial fit to data ≥7000 eV. The data were then divided by the absorption for a free atom.[19]

For analysis, the data were transformed to a function of the wave vector k where, for the threshold energy for photoionization E_0, $k = [(E-E_0)2m_e/h^2]^{1/2}$. The Fourier transform of the k-space data gives peaks appearing at $R' = (R + \Psi/2)$ representing shells of scatterers at average distances R from the absorbing Mn. Due to the phase shift, the apparent distance R' is generally less than R by 0.2–0.5 Å.

Curve-fitting analysis was performed on Fourier-filtered k-space data. Fourier filtering was performed by applying a square-window function over regions of the Fourier-transformed data and back-transforming to k space. These data were windowed and fit as pairs of Fourier transform peaks; i.e., peaks (I and II) (0.3 Å ≤ R' ≤ 3.0 Å) or peaks (II and III) (1.8 Å ≤ R' ≤ 4 Å) were isolated and back-transformed for fitting. Fits were also performed on the isolated peak (III) (2.5 Å ≤ R' ≤ 3.5 Å). This method was chosen to avoid potential artifacts induced by the windowing function[20] and to reduce correlation between fitting parameters by providing comparisons between multiple combinations of data.

Two methods of low-frequency background subtraction were tested before conversion of the data from energy to a function of photoelectron wave vector k. Either a second-order polynomial fit to the data (≥7000 eV) or a two-domain spline fit to the data (≥6600 eV) was subtracted. After conversion of the data to a function of k, a three-domain spline was subtracted from data which had been treated with a polynomial fit. The success of background subtraction was judged by inspecting the unwindowed Fourier transform of the k-space data for minimization of peak amplitude at $R' \leq 1$ Å. The spline removal in energy space generally gave cleaner Fourier transform spectra, but both methods of background subtraction resulted in similar parameters in the fitting analysis.

The data were fit to eq 2 using the program EXFIT[18] as described.[4] For a shell j of scatterers, N_j is the number of a given type of scatterer and R_j is the absorbing atom–scatterer distance.

$$\chi(k) = \sum_j \frac{N_j}{kR_j^2} |f_j(k,\pi)| \sin[2kR_j + \Psi_j(k)] e^{-2\sigma_j^2 k^2} \quad (2)$$

For these data, theoretical atomic phase (Ψ_j) and scattering amplitude (f_j) functions were used which had been calculated using curved-wave approximations.[21] Additional calculations were performed using the program FEFF 3.0.[22] The fit results were judged by the sum of residuals between the simulated and real data multiplied by k^x where x is the k-weighting factor.

The analysis of each shell j of scatterers involves four variable parameters: N_j, R_j, σ^2, ΔE. The values for σ^2, the Debye–Waller disorder parameter, and ΔE, a variable E_0, were constrained to ranges indicated by fits to representative model compounds, and N and R were refined for each shell. This restricted fit methodology, based on the "fine adjustment based on models" method,[23] was described for Mn model compounds by Guiles et al.[4c,d] Constraints in parameters for the short Mn–oxo and terminal ligand shells as well as the Mn–Mn distance at 2.7 Å were taken from that work. These parameters were found to be satisfactory for the analysis of model compound data taken at 10 K. For the longer Mn–Mn interactions, values of σ^2 and ΔE were determined from model compound data presented here.

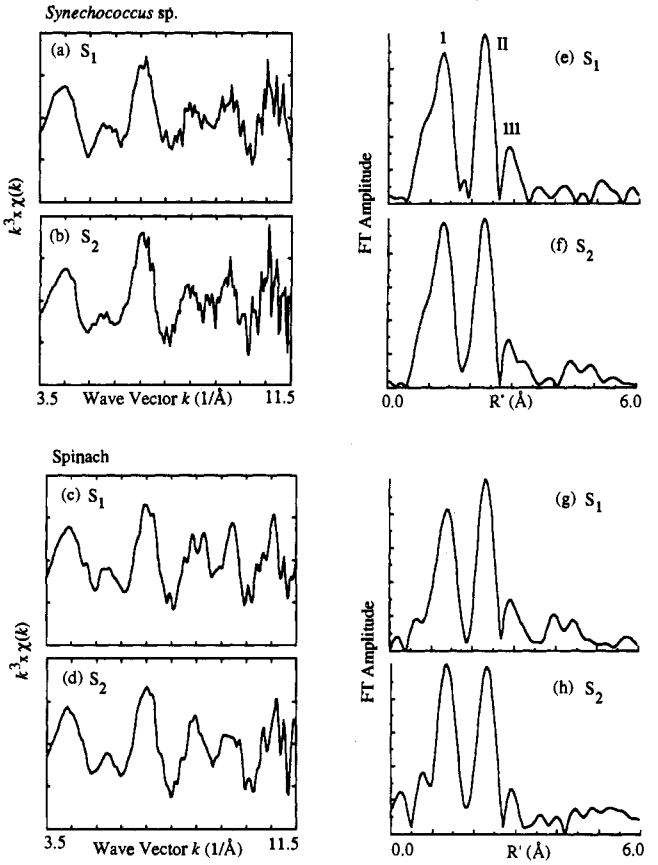

Figure 1. Mn K-edge EXAFS data for *Synechococcus* sp. and spinach photosystem II preparations poised in the S_1 and S_2 states. The data shown are weighted by k^3. The k-space data for (a, b) *Synechococcus* sp. S_1 and S_2 and (c, d) spinach S_1 and S_2 samples are plotted. The Fourier transforms of the unwindowed k-space data for (e, f) *Synechococcus* S_1 and S_2 and (g, h) spinach S_1 and S_2 samples are also shown. The data are normalized and treated as described in the text under Methods. The vertical scales for all k-space data are ±7.5 and for all Fourier transforms are 0.0–0.25 (au).

Results

Low-Temperature Mn EXAFS of PSII Samples. The Mn EXAFS from a *Synechococcus* and a spinach PSII preparation poised in the S_1 and S_2 states are presented in Figure 1a–d. The k^3-weighted traces in Figure 1 show improved signal to noise

(17) Cramer, S. P.; Tench, O.; Yocum, M.; George, G. N. *Nucl. Instrum. Methods Phys. Res.* **1988**, *A226*, 586.
(18) Goodin, D. B. Ph.D. Dissertation, University of California—Berkeley, 1983; Report LBL-16901; Lawrence Berkeley Laboratory: Berkeley, CA, 1983.
(19) McMaster, W. H.; Kerr Del Grande, N.; Mallett, J. H.; Hubbell, J. H. Compilation of X-ray Cross Sections. Report UCRL-50174; Lawrence Berkeley Laboratory: Berkeley, CA, 1969.
(20) Zhang, K.; Stern, E. A.; Ellis, F.; Sanders-Loehr, J.; Shiemke, A. K. *Biochemistry* **1988**, *27*, 7470–7479.
(21) McKale, A. G.; Veal, B. W.; Paulikas, A. P.; Chan, S.-K.; Knapp, G. S. *J. Am. Chem. Soc.* **1988**, *110*, 3763–3768.
(22) Rehr, J. J.; Mustre de Leon, J.; Zabinsky, S. I.; Albers, R. C. *J. Am. Chem. Soc.* **1991**, *113*, 5135–5140.
(23) Teo, B. K.; Antonio, M. R.; Averill, B. A. *J. Am. Chem. Soc.* **1983**, *105*, 3751–3762.

Table 1. EXAFS Fit Parameters for S_1 and S_2 Preparations for Peaks (I and II)

sample	atom	R (Å)[a]	N[b]	$2\sigma^2 \times 10^3$ (Å^2)	fit error
Synechococcus S_1 [A][c]	O	1.81	2.0	7	31
	Mn	2.74	1.4	9	
[B]	O	1.79, *1.80*[d]	1.3, *1.8*	2	25, *24*
	O(N)	1.98, *1.90*	0.4, *4.6*	2, *11*	
	Mn	2.74	1.4	5	
[C]	O	1.81	2	2	27
	O(N)	1.90	4	10	
	Mn	2.74	1	5	
spinach S_1 [A]	O	1.86	2.2	9	34
	Mn	2.74	1.6	9	
[B]	O	1.80, *1.81*	1.2, *2.4*	2	20, *17*
	O(N)	1.96, *1.90*	0.8, *4.8*	2, *7*	
	Mn	2.74	1.2	5	
[C]	O	1.81	2	2	19
	O(N)	1.90	4	7	
	Mn	2.74	1	5	
Synechococcus S_2 [A]	O	1.83	2.5	10	80
	Mn	2.74	1.5	8	
[B]	O	1.79, *1.81*	1.5, *2.2*	2	48, *52*
	O(N)	1.98, *1.90*	0.8, *5.0*	2, *9*	
	Mn	2.74	1.2	5	
[C]	O	1.81	2	2	58
	O(N)	1.90	4	9	
	Mn	2.74	1	5	
spinach S_2 [A]	O	1.86	2.5	10	75
	Mn	2.73	1.1	9	
[B]	O	1.80, *1.82*	1.4, *2.3*	2	42, *36*
	O(N)	1.98, *1.91*	0.8, *5.0*	2, *8*	
	Mn	2.73	1.2	5	
[C]	O	1.82	2	2	45
	O(N)	1.91	4	8	
	Mn	2.73	1	5	

[a] Variables used in the fits are described in the text and are as follows: R, average distance from absorbing Mn of atoms in scattering shell; N, number of scatterers at distance R; σ, Debye–Waller disorder parameter; fit error, least-squares difference between data and calculated fit. Parameter errors (variability in parameters giving 10% rise in fit error): R, ±0.02 Å; N, ±30%. [b] The number N of scatterers is derived by multiplication of the fit values by a factor of 2.[3,21] [c] Fit [A] is a two-shell fit to the data. Fit [B] is a three-shell fit with no constraints on the coordination numbers for each shell. In fit [C], the total number of ligands on Mn is constrained to 6. For all fits, -20 eV $\leq \Delta E \leq 5$ eV. For fits [B] and [C], σ^2 is constrained for the Mn shell. [d] Parameters in italics indicate a second local minimum in fit error for unconstrained fits [B]. These fits predict differences in R that are smaller than the theoretical resolution of ~0.12 Å of this experiment.[3d]

ratio as compared with previous data for these types of preparation.[4a–d] The Fourier transforms of these data in Figure 1e–h show three main peaks, labeled I-III. While peaks I and II are similar to previous data taken at sample temperatures of 180 K, peak III at $R' = 2.9$ Å was not reliably observed in data taken at the higher temperature[4d] but here is clearly above the noise level (as measured by the average peak amplitude at $R' >$ 5 Å) in both types of preparations.

In addition, small but consistent changes are seen between samples poised in the S_1 and S_2 states. These differences appear as changes in the relative amplitudes of the Fourier transform peaks I and II and appear in both S_1 and S_2 pairs displayed here as well as in other data sets (not shown).

Analysis of Peaks (I and II). The fit parameters for these shells are given in Table 1. These data were first fit to two shells of scatterers, one of light (O, N) and one of heavy (Mn, Fe) atoms. When only two shells are used (fit A in Table 1), the minimum in fit error is always found for a short light atom scatterer at <1.9 Å and a heavy atom scatterer at ~2.7 Å distance from the absorbing Mn. The short Mn–O distance is representative of μ-oxo bridges in Mn model compounds.[6] As has been previously discussed,[1c] while EXAFS cannot be used to judge between elements of similar Z, a variety of other physical evidence indicates that Mn is the partner at the 2.7-Å distance. It is clear from these fits that the dominant contributions to these data are fit well by a combination of (per Mn) ~2 O scatterers at 1.8 Å and ~1 Mn scatterer at 2.7 Å. The coordination numbers and Debye–Waller factors for these shells are not significantly different from our previous data of this type.

Attempting to model a disordered terminal ligand shell by the addition of a third shell of light atoms (O, N) to fit this isolate reduces the fit error by ~20–50%. Two types of fits including a terminal ligand shell are given in Table 1. The first fit (fit B) has no constraints on the number of terminal ligands. This type of fit generally results in a fit with either coordination numbers of <6 per Mn or a very short terminal ligand distance (Table 1, italics). This behavior likely indicates that a single shell does not adequately describe the terminal ligand scatterers. As has been previously discussed,[3d] for an unknown system the distance and coordination number determination by EXAFS of highly disordered shells of scatterers is subject to increased error. This is due to the inability of a single Debye–Waller parameter to describe the disordered shell. The effect is compounded when a single scattering shell contains unresolved components, of which one (in this case, the bridging O) is the dominant interaction. The terminal ligand shell in a mixed-valent multinuclear Mn compound is expected to contain a mixture of distances: excluding bridging O atoms, ligand distances in compounds containing Mn(III) and Mn(IV) range from 1.9 to 2.2 Å depending on oxidation state and type of ligand.[6,12–16] A third type of fit (fit C in Table 1) was included in which the number of ligand scatterers was held to a total of 6 per Mn. The combination listed of 2 O at 1.8 Å and 4 terminal ligands gave the lowest fit errors for this type of fit.

For both of these types of fits, a relatively short average Mn–terminal ligand distance of <~2.0 Å is favored for the OEC. This is shorter than the value of ~2.2 Å that has been reported previously for these preparations.[4b,c] Fits performed on peak I only (data isolated in the range 0.5 Å $\leq R' \leq$ 2.0 Å) do have a lower fit error for a second shell of scatterers at ~2.2 Å in addition to the 1.8-Å shell (data not shown), but the fits described above to the *combined* peaks (I and II) show a preference for the shorter R values. It could be that peaks I and II are not adequately resolved to avoid Fourier transform windowing artifacts that, when the first peak is isolated alone, influence the determination of these longer distances.

Compared with the bridging O atom scatterers at $R_{av} \sim 1.8$ Å, the terminal ligand shell makes a very weak contribution to the PSII EXAFS. The relative contributions of the 1.8– and 1.9–2.0-Å shells are further emphasized in Figure 2. This figure shows the Fourier transforms of each individual fit shell. It is clear that the original EXAFS data contributing to peaks I and II are nearly replicated with the shells of atoms at 1.8 and 2.7 Å, while the ≥1.90-Å shell makes only a small contribution to the overall EXAFS.

Chloride has been implicated as a cofactor of oxygen evolution. Mn–Cl bond distances of 2.2–2.6 Å are found in Mn(III) and Mn(IV) compounds.[24] Including a shell of Cl in the analysis gave ambiguous results. It was possible to model the effects of the terminal ligand shell in the fit of peaks (I and II) by a single shell of Cl; i.e., fits including *either* Cl, at a relatively short distance of ~2.2 Å, *or* the (O, N) terminal ligand shell described above gave comparable fit errors (not shown). As found by previous investigators,[4b,8b] however, the more realistic scenario consisting of the addition of a single Cl scatterer to the fit already including both bridging and terminal (O, N) ligands did not result

(24) Pecoraro, V. L.; Butler, W. M. *Acta Crystallogr., Sect. C* **1986**, *C42*, 1151–1154. See also refs 14 and 28 in this paper.

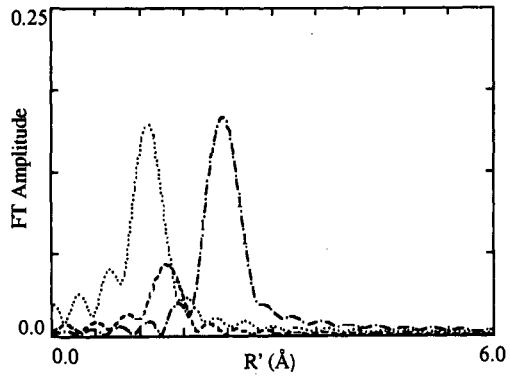

Figure 2. Decomposition of EXAFS fits for peaks (I and II). The individual shells of fit [B] (Table 1) for the *Synechococcus* sp. S_1 data set are shown as their respective Fourier transforms. The represented shells are bridging O (1.79 Å, dotted line), terminal ligand O, N (1.98 Å, dashed line), and Mn (2.7 Å, dash–dot line).

in a significant improvement of fit error and so cannot be justified.

The data analysis used here depends on approximated photoelectron backscattering and phase shift functions,[21] and while it correctly predicts short shell distances in model compounds, we have also tested our results using a more exact calculation. The program FEFF[22] performs *ab initio* atomic potential calculations for an atom with a chosen nearest set of neighbors. Using this method, we calculated phase and amplitude functions for a model of Mn with average oxidation state of 3.5 and average number of 2 O(N) neighbors at a distance of 1.8 Å. Analysis of the first-shell OEC EXAFS using these calculated functions (data not shown) gave parameters nearly identical to those from the fits performed with the tabulated functions calculated using the curved-wave approximation.[21]

Analysis of Scatterers at >3 Å. The Fourier transform peak at $R' \sim 3$ Å reflects scattering from atoms at distances greater than 3 Å from the absorbing Mn atoms. To model these contributions, data from both the isolated Fourier transform peak III and a combination of peaks (II and III) were analyzed. Combinations of Mn, Ca, and C were tested to model the longer distance interaction. Distances of 3.1–3.4 Å are found between Mn atoms bridged by a single μ_2- or μ_3-oxo unit.[6] In addition, for carboxylate- or histidine-derived ligands a highly disordered shell of C atoms at ~2.9–3.3 Å may be expected from the atoms two bonds from the metal. The Debye–Waller parameter for this type of C shell was constrained to ≥0.01 Å^2 to reflect the expected disorder, especially given the disorder of the primary ligand atoms in this system as indicated by the small contribution of the terminal ligands in the OEC EXAFS (Figure 2). Ca was included in the fit combinations because it has been implicated through activity and EPR experiments as a possible structural component of the OEC,[1a] and replacement with Sr has been found to alter the apparent amplitude of peak III.[4e,25]

The fit parameters for the isolated peak III are shown in Table 2. A single-shell fit of the isolated peak gives a lowest fit error for Mn as the scattering atom in all cases. The fit error is nearly twice as high for Ca and much greater for a single shell of C. The addition of a second shell of scatterers significantly decreases (by ~80% in some cases) the fit error for this peak. The fit errors for the two-shell fits are lowest for combinations of Mn/C and Mn/Ca and higher for Ca/C.

The fit parameters for data contributing to Fourier transform peaks (II and III) are listed in Table 3. To reduce the contribution from O, N, or C light atom scatterers, whose amplitude scattering functions maximize at lower k values than do those of heavier scatterers such as Mn or Ca, these data were fit over a higher k range (~4.5–11.8 Å^{-1} as opposed to 3.5–11.8 Å^{-1} for peaks (I and II));[20] similar results were found, however, for the full-range data. The parameters for single- and two-shell fits to this isolate are tabulated for *Synechococcus* and spinach OEC preparations. The 2.7-Å scatterers are the dominant contribution to these peaks, but the additional shell of scatterers at ~3.3 Å decreases the fit error by >80% in the S_1 data sets. Parameters describing the best fits of these combinations are shown in Table 3. In contrast to the fits to the isolated peak III, these fits did not show a clear discrimination between types of scatterers at >3 Å, although the relatively large number of C scatterers required at that distance (~3 per Mn at ~3.4 Å) seems unlikely given the disorder of the ~2-Å terminal ligand shell. The addition of a third shell of scatterers did not show a significant decrease in fit error for this data combination.

Comparison of Fit Model to Raw EXAFS Data. The fits described above were performed on data isolated as individual peaks from the Fourier transform of the raw EXAFS data, and back-transformed to k-space. This procedure is performed both in order to remove high-frequency noise from the data and to fit individual scatterer shells or sets of shells. To check the validity of the model derived from the fitting analysis of isolated data, global fits to an isolate including peaks I–III (0.5 Å ≤ R' ≤ 3.5

(25) Latimer, M. J. Personal communication.

Table 2. EXAFS Fit Parameters for Peak III[a]

sample	atom	R (Å)	N	$2\sigma^2 \times 10^3$ (Å^2)	fit error (×10^2)
Synechococcus S_1	Mn	3.36	0.6	10	29
	Ca	3.41	0.6	6	53
	C	3.39	2.8	10[b]	380
	Mn	3.32	0.3	4	7
	C	3.42	1.4	10	
	Ca	3.34	0.3	2	11
	C	3.42	1.8	10	
	Mn	3.31	0.3	6	6
	Ca	3.42	0.7	15	
Synechococcus S_2	Mn	3.36	0.4	3	9
	Ca	3.41	0.4	2	41
	C	3.38	2.2	10	600
	Mn	3.35	0.4	4	2
	C	3.48	0.8	10	
	Ca	3.39	0.6	3	5
	C	3.38	1.1	10	
	Mn	3.33	0.4	2	2
	Ca	3.37	0.6	11	
spinach S_1	Mn	3.39	0.6	5	72
	Ca	3.44	0.6	2	160
	C	3.42	2.2	10	300
	Mn	3.38	0.6	9	10
	C	3.10	0.6	10	
	Ca	3.42	0.6	5	30
	C	3.10	0.6	10	
	Mn	3.32	0.3	5	19
	Ca	3.44	0.6	9	
spinach S_2	Mn	3.36	0.3	6	19
	Ca	3.41	0.3	3	29
	C	3.39	1.8	10	215
	Mn	3.33	0.4	5	3
	C	3.25	1.2	10	
	Ca	3.37	0.6	5	9
	C	3.26	2.0	10	
	Mn	3.38	0.3	4	33
	Ca	3.39	0.3	15	

[a] Errors, coordination numbers, and constraints on ΔE are as described in Table 1. [b] $2\sigma^2$ was constrained to 0.010 Å^2.

Table 3. EXAFS Fit Parameters for Peaks (II and III)[a]

sample	atom	R (Å)	N	$2\sigma^2 \times 10^3$ (Å^2)	fit error
Synechococcus S_1	Mn	2.71	1.0	4	32
	Mn	2.71	0.9	4	5
	Mn	3.36	0.6	10	
	Mn	2.71	0.8	3	3
	Ca	3.42	0.6	10	
	Mn	2.70	0.8	2	3
	C	3.37	3.0	10	
Synechococcus S_2	Mn	2.72	1.2	5	29
	Mn	2.71	1.2	5	12
	Mn	3.34	0.4	10	
	Mn	2.71	1.2	5	10
	Ca	3.38	0.6	10	
	Mn	2.71	1.0	4	12
	C	3.32	2.2	10	
spinach S_1	Mn	2.73	1.2	4	39
	Mn	2.73	1.2	4	7
	Mn	3.42	0.4	5	
	Mn	2.73	1.0	4	7
	Ca	3.46	0.6	5	
	Mn	2.73	1.0	3	12
	C	3.41	2.2	10	
spinach S_2	Mn	2.71	1.2	5	15
	Mn	2.71	1.2	5	9
	Mn	3.39	0.3	10	
	Mn	2.71	1.2	5	9
	Ca	3.43	0.4	10	
	Mn	2.71	1.2	5	10
	C	3.36	1.4	10	

[a] Coordination numbers, fit errors, and constraints on ΔE are as described in Table 1.

Å) were performed and compared to the original data. These global fits included the following scattering shells: O (~1.8 Å), O(N) (≥1.9 Å), Mn (~2.7 Å), Mn (~3.3 Å). The comparison of these fits to the original EXAFS data of *Synechococcus* S_1 and S_2 samples is shown in Figure 3. It can be seen that both the isolated data and the resulting fits to the isolated data mimic the raw EXAFS data quite well.

Differences between the S_1 and S_2 States. In Figure 4 the Fourier transforms of data taken on spinach and *Synechococcus* preparations poised in the S_1 and S_2 states are overplotted. These data show small but consistent changes in the relative amplitudes of the Fourier transform peaks I and II between samples poised in the different S states. These differences are slight, but they are detected in multiple data sets from different organisms. The small changes in the relative amplitudes of the Fourier transform peaks in these data are not reflected by the fit parameters listed in Table 1 for peaks (I and II). Of note, however, the fit *errors* for the S_2 state data are higher than those for the S_1 state, despite similar signal to noise ratios in the EXAFS data. This indicates that the three-shell fit may not adequately model the S_2 state data. Including a fourth shell of scatterers, however, did not decrease the fit error significantly.

EXAFS Data of Mn Model Compounds. EXAFS data from several Mn model compounds containing Mn–Mn distances of ~2.7 and/or >3 Å were also analyzed in order to compare them with the OEC EXAFS, as well as to investigate the ability of EXAFS to identify interactions at longer distances in multinuclear Mn compounds and to determine reasonable ranges for the EXAFS fit parameters for the unknown OEC structure. The cores of the models used are depicted in Figure 5 and include $[Mn^{III}_2(O(OAc)_2)]$ (**1**, "dimer"), $[Mn^{III}_3(O(C_6H_5CO_2)_6)]$ (**2**, "symmetric trimer"), $[Mn^{IV}_3O_4]$ (**3**, "asymmetric trimer"), $[Mn^{III}_4(O_2(OAc)_7)]$ (**4**, "butterfly"), and $[Mn^{III}_3Mn^{IV}(O_3Cl)]$ (**5**, "asymmetric tetramer").

Table 4. EXAFS Fit Parameters for Multinuclear Mn Model Compounds[a]

model	atom	R (Å)	N	$2\sigma^2 \times 10^3$ (Å^2)	fit error
dimer (**1**)	Mn	3.12 (3.08)[b]	1.2 (1)	9	1
	C	3.39[c]	3.0	15	
	Mn[d]	*3.13*	*0.8*	*8*	*1*
	Ca	*3.18*	*0.7*	*4*	*3*
	C	*3.16*	*3.0*	*8*	*19*
symmetric trimer (**2**)	Mn	3.28 (3.27, 3.26)	1.7 (2)	12	6
	C	2.92	1.6	2	
asymmetric trimer (**3**)	Mn	3.24 (3.24)	1.7 (1.3)	3	16
	Mn	2.78 (2.68)	1.0 (0.7)	2	
	C	3.7	1.8	2	
butterfly (**4**)	Mn	3.41 (3.34)	1.0 (2)	7	0.4
	C	2.86	0.3	20	
asymmetric tetramer (**5**)	Mn	2.85 (2.80)	1.5[e]	2	7
	Cl	2.61 (2.65)	0.7	2	
	Mn	2.99 (3.25)	1.5	4	
	Mn	*2.84*[d]	*1.9*	*7*	*147*
	Mn	*2.89*	*2.5*	*15*	*30*
	Cl	*2.60*	*0.8*	*2*	
	Mn	*2.80*[f]	*1.5*	*6*	*12*
	Cl	*2.65*	*0.7*	*2*	
	Mn	*3.25*	*1.5*	*11*	

[a] Fit errors, values for N, and constraints for ΔE are as described in Table 1. [b] Crystallographic parameters for R and N are in parentheses. [c] Several shells of low-Z scatterers contribute at a range of distances ≥3 Å in these compounds.[26,29] The distance for this C shell was not well constrained in these fits; i.e., for a given shell of Mn, two or more different distances for the C shell gave fit errors within 10%. [d] Additional fit parameters in italics are given in order to describe the behavior of these compounds, as explained in the text. [e] Values for N were constrained to the crystallographic parameters in these fits. [f] Values for N and R were constrained to the crystallographic parameters in these fits (see text).

The Fourier transforms of these model compounds are compared with the OEC data in Figure 6. Qualitatively, it can be seen that the influence of multiple metal–metal and terminal ligand distances can complicate the EXAFS data of these model compounds. The amplitudes of the peaks at $R' \sim 2.9$ Å that correspond to the Mn–Mn scatterers at >3 Å do not always scale in a simple way with the number of interactions at >3 Å. For example, compound **1** (dimer) has 1 metal scatterer (per Mn) at 3.1 Å and **2** (symmetric trimer) and **4** (butterfly) have 2 scatterers (per Mn) near this distance. The amplitudes of their FT peaks at $R' \sim 3$ Å scale accordingly. Despite having only 1.3 Mn–Mn scatterers at >3 Å, however, compound **3** (asymmetric trimer) has a peak at $R' \sim 3$ Å with an amplitude similar to those for **2** and **4**. Compound **5**, the "asymmetric tetramer", does not show a resolved peak for its 1.5 Mn–Mn scatterers per Mn at ~3.3 Å (Figure 7).

The k-space data corresponding to the isolated peaks resulting from >3-Å scatterers in **1**, **2**, and **4** are compared to the OEC data in Figure 8. For **3** and **5** it was not possible to isolate the peak due to >3-Å scatterers (see below). The data were treated as similarily as possible to the OEC data with respect to background subtraction and Fourier filtering. The fit parameters are listed in Table 4, and the best fits are plotted over the data in Figure 8. Agreement is found between parameters determined from the EXAFS fits and the distances and coordination numbers expected from X-ray crystal structures (in parentheses in Table 4) for both **1** and **2**, within error of ±0.04 Å and 30%, respectively. This is highly encouraging, given the complexity of the models and the presence of terminal ligand atoms at distances close to

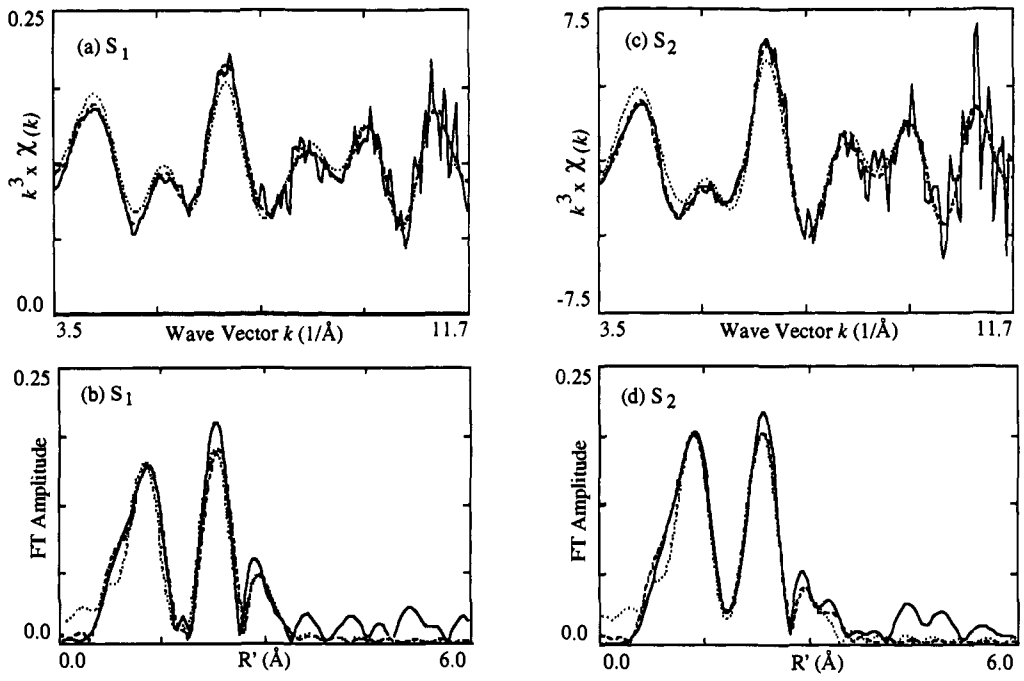

Figure 3. Comparison of fit model and isolated data for raw EXAFS. Three-shell isolates (0.5 Å ≤ R' ≤ 3.5 Å) (dashed lines) and fits to those isolates (dotted lines) are plotted over the raw data (solid lines) shown in Figure 1 for *Synechococcus* sp. S_1 and S_2. The k-space data (a, c) are shown as well as the resulting Fourier transforms (b, d). The global fits shown in dotted lines include four shells, described in the text, that have parameters nearly identical to the combinations of fit [C] in Table 1 and the first listing in Table 2 for each data set.

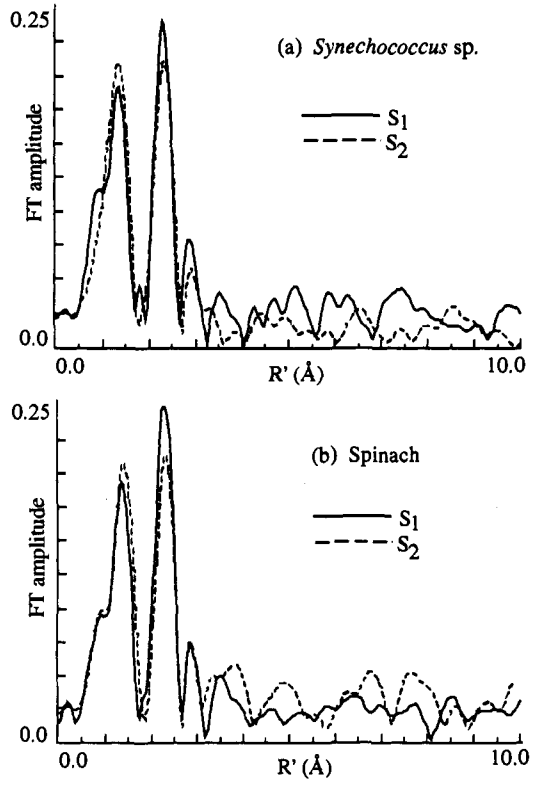

Figure 4. Comparison of Mn EXAFS data for PSII preparations poised in the S_1 and S_2 states. The Fourier transforms from samples in the S_1 (solid line) or the S_2 (dashed line) state are overplotted for (a) *Synechococcus* sp. and (b) spinach PSII preparations.

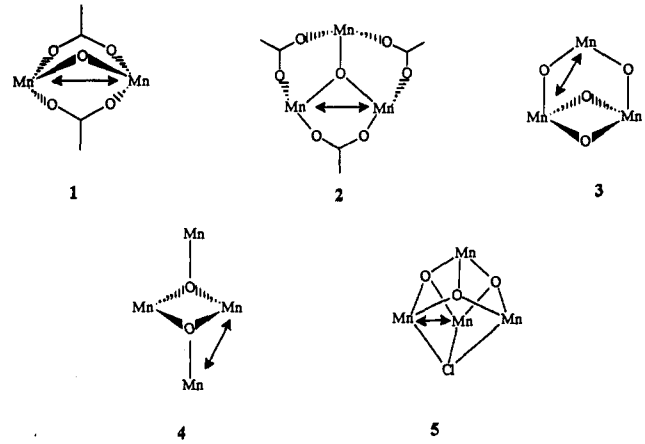

Figure 5. Schematic diagrams of the model compounds used in this study. For simplicity, only Mn and the bridging ligand atoms are shown. The complexes are described in the text and are denoted as dimer (**1**), symmetric trimer (**2**), asymmetric trimer (**3**), butterfly (**4**), and asymmetric tetramer (**5**). For convenience, only one of the two carboxylate bridges between Mn atoms are shown for compound **2**. The arrows indicate >3-Å Mn–Mn distances.

those of the ~3-Å Mn scatterers.[26] As shown in Table 4, attempts to fit the dimer model (incorrectly) to single shells of Ca or C gave increasing fit errors, similar to the behavior of peak III of the OEC data (Table 2). For the "butterfly" compound (**4**), whose four long Mn–Mn distances can be grouped into two shells at average distances of 3.3 and 3.4 Å, the isolated Fourier transform peak at R' = 3 Å fits well to a single shell of Mn at an average 3.4-Å distance. It is possible that one shell of Mn scatterers at this distance is too disordered to be detected.

Unlike that of the butterfly model, the Fourier transform of the asymmetric trimer (**3**) does not show resolution between the $^2/_3$ scatterer per Mn at 2.7 Å and $^4/_3$ scatterers per Mn at 3.2 Å. In this compound, each Mn has several neighboring N atoms from bipyridyl ligands, as well as a terminal Cl ligand at 2.3 Å for two of the Mn. The range of distances for these interactions and additional potential multiple scattering effects from bipy[27] greatly complicate the analysis of this compound. The data isolated for R' = 2–4 Å are shown in Figure 8e. These data were

(26) Hedman, B.; Co, M. S.; Armstrong, W. H.; Hodgson, K. O.; Lippard, S. J. *Inorg. Chem.* **1986**, *25*, 3708–3711.

(27) Strange, R. W.; Blackburn, N. J.; Knowles, P. F.; Hasnain, S. S. *J. Am. Chem. Soc.* **1987**, *109*, 7157–7162.

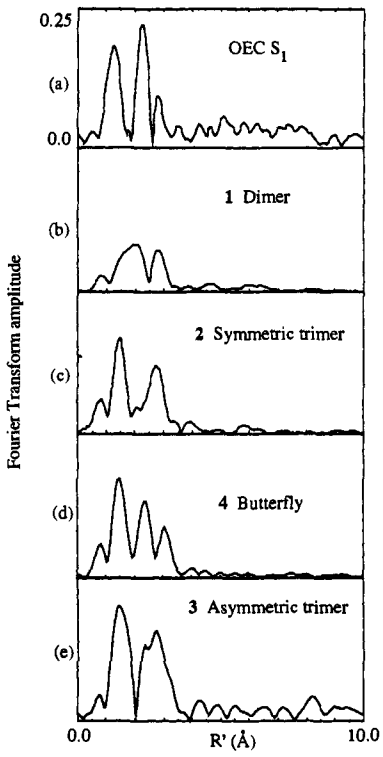

Figure 6. Comparison between the Mn EXAFS data from the OEC and multinuclear Mn model compounds. The Fourier transforms of Mn EXAFS k-space data (3.5–11.5 Å^{-1}) are shown for (a) *Synechococcus* sp. poised in the S_1 state and (b–e) the model compounds depicted in Figure 5. The data are normalized as described in the text under Methods, and the vertical axes in each case are 0.0–0.25 (au).

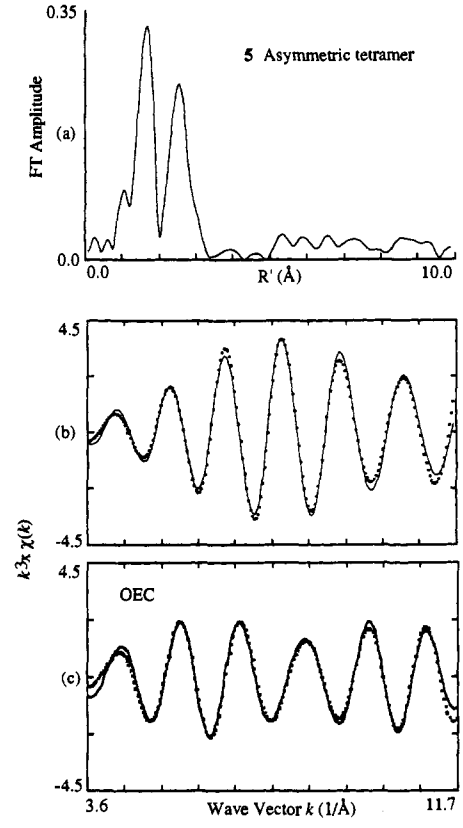

Figure 7. Mn EXAFS data for model compound **5**. (a) The Fourier transform of unwindowed Mn EXAFS k-space data (3.7–11.7 Å^{-1}) from **5** is shown. Note that the vertical axis of 0.0–0.35 (au) for the Fourier transform amplitude is greater than the scale of 0.0–0.25 (au) used for all plots in Figure 6. (b) Fourier-filtered k-space data (solid line) of the isolated second peak (1.8 Å $\leq R' \leq$ 3.5 Å) from **5** are shown. The analytical fit (Table 4, last listing) is also shown (dotted line). (c) Fourier-filtered k-space data of the same R' region from a *Synechococcus* sp. S_1 preparation (solid line), including peaks (II and III) (1.8 Å $\leq R' \leq$ 3.5 Å), are shown. The analytical fit from Table 3 (second listing) is overplotted (dotted line).

fit to Mn at 2.8 and 3.2 Å and to a terminal ligand shell of scatterers. While this fit is clearly of much poorer quality than for the other models, the number and distance of Mn scatterers at 3.2 Å are adequately modeled.

Compound **5** is a highly distorted cubane model with a μ_3-Cl atom substituting the bridging position of one O atom. The model is intriguing for several reasons and has been proposed as a model for the OEC in the S_2 state.[16,28] It is unique in its incorporation of Cl into a tetranuclear Mn cluster and has relatively long Mn(III)–Cl distances of ~2.6 Å. That distance is very close to the 2.8-Å Mn–Mn distance found in this cluster and to the 2.7-Å Mn–Mn distance in the OEC, and it is interesting to note its effects on the ability to analyze the Mn–Mn interactions by EXAFS. In addition, the model has (per Mn) 1.5 Mn–Mn interactions at ~3.3 Å. These result in a shoulder on the R' ~ 2.5 Å peak but not a resolved peak in the Fourier transform (Figure 7).

These scattering interactions from **5** were isolated as a single peak (Figure 7b), R' = 1.8–3.5 Å, and the resulting fit parameters are listed in Table 4. Attempting to model these unresolved interactions as a single shell of Mn scatterers results in a very poor fit to the isolated data and gives an average Mn–Mn distance of 2.84 Å (R_{av}(crystallography) = 2.795 Å). Addition of a shell of Cl scatterers reduces the fit error by 80%. The Mn–Cl parameters of 0.8 Cl scatterer at 2.60 Å compare favorably with the expected 0.75 scatterers at 2.65 Å in these two-shell fits. As expected, given the different backscattering phase and amplitude functions for Mn and Cl, it was not possible to simulate the data mistakenly with a second shell of Mn at or near this distance. Although a similar fit error could be attained by adding an additional shell of Mn, this fit required unrealistically high numbers of scatterers (~5 each) for each Mn shell (data not shown).

For this model compound, the 1.3 Mn–Mn interactions at ~3.3 Å were not easily determined by the EXAFS fit analysis. The addition of a third shell of Mn scatterers at >3 Å does reduce the fit error by another 60%. It was found, however, that unless it was restricted, the long Mn–Mn distance expected at 3.25 Å refined to the much shorter distance of 2.99 Å. In these fits the 2.8-Å Mn–Mn distance and the 2.6-Å Mn–Cl distance refined to the same parameters as for the two-shell fit. When the distance and coordination number parameters for all three shells were held to their crystallographic values, however, the fit error was still decreased by a factor of 2 over the two-shell fit (Table 4, and shown in Figure 7). This appears to be an example in which the multitude of terminal ligands having atoms at distances of R ~ 2.9–3.0 Å interfere with the analysis by EXAFS of the long-distance metal–metal interactions. The 2.6-Å Mn–Cl bond was modeled well in the EXAFS analysis, however, and did not significantly interfere with analysis of the 2.8-Å Mn–Mn interactions.

While it was difficult to uniquely model by EXAFS the number of scatterers at ~3.3 Å in complex **5**, it is important to note that the EXAFS data of this complex have substantial dissimilarities from those of the OEC. This is seen in the amplitude of the Fourier transform peaks (note the scale in Figure 7) and also in the comparison of the Fourier-filtered data. Differences are seen in the Fourier-filtered data, compared in Figure 7, of the contributions of the scatterers at 2.7–3.3 Å of both the OEC and the asymmetric tetramer **5**. The OEC EXAFS feature due to scatterers at ~3.3 Å appears to be more closely approximated

(28) Hendrickson, D. N.; Christou, G.; Schmitt, E. A.; Libby, E.; Bashkin, J. S.; Wang, S.; Tsai, H.-L.; Vincent, J. B.; Boyd, P. D. W.; Huffman, J. C.; Folting, K.; Li, Q.; Streib, W. E. *J. Am. Chem. Soc.* **1992**, *114*, 2455–2471.

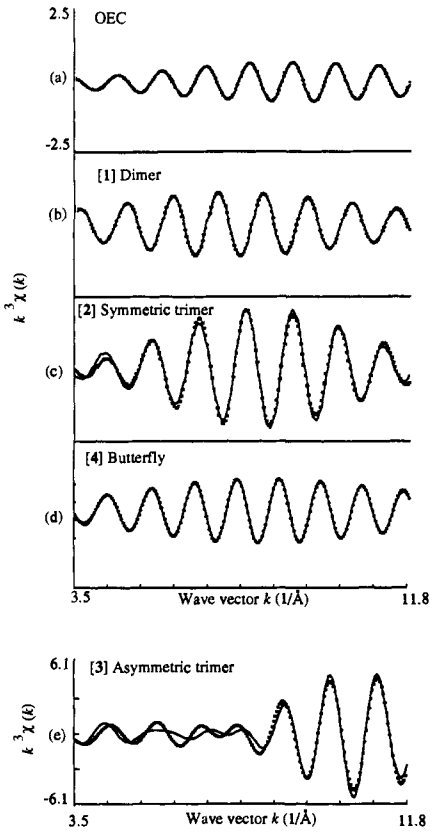

Figure 8. Analytical fits to the Fourier-filtered k-space data including Mn–Mn interactions at >3 Å in the OEC and Mn model compounds. Fourier-filtered data (solid lines) of isolated Fourier transform peaks at $R' \sim 2.9$ Å are shown for (a) the *Synechococcus* sp. S_1 and (b–d) the model compound data described by Figure 6. The data for (e) 3 include Mn scatterers at both 2.7 and ~3.3 Å, as described in the text. Analytical fits (dotted lines) are plotted over the k-space data. Parameters for each fit are described in the text and in Table 4.

by the dimer **1** (see Figures 6 and 8), whose features are successfully modeled by the EXAFS analysis.

Discussion

First Scatterer Shell. There have been disparate reports concerning the presence of short bridging ligands in the OEC. EXAFS analysis of bridged model compounds has been quite successful in discriminating between ligand distances of 1.8 and 1.9 Å and thus distinguishing between, for example, μ-oxo and μ-hydroxo bridges.[4c,d,20,26,29] In these OEC data, analysis of the first shell of light-atom scatterers indicates that each Mn has 2 ± 0.5 neighboring atoms at the relatively short distance of 1.80–1.84 Å. This result is model-independent; i.e., fits using both the theoretical phase and amplitude functions tabulated for isolated atoms[21] and phase and amplitude functions calculated using model-dependent atomic potentials[22] give identical results. Our results for this shell agree with those arrived at by MacLachlan et al.[8c] for both spinach BBY preparations and the detergent-solubilized "HTG" preparations. Our disagreement with the results of Penner-Hahn et al.[8b] and George et al.,[8a] who report longer average bond distances, is most likely due to the skewing of their first-shell EXAFS analysis by the presence of contaminating Mn^{2+}.[1a,30]

The relatively small contribution from the other, terminal ligands around Mn in the OEC, which from comparison with model compounds would give rise to scattering at 1.9–2.2 Å, indicates as expected that these ligands are highly disordered. Our results are again in agreement with those of MacLachlan et al.[8c] in finding a relatively short average terminal ligand distance of <2 Å. In high-valent Mn(III)/Mn(IV) model compounds, the Mn–terminal ligand distances for N-donor ligands are *on average* slightly longer than Mn–O distances for, e.g., carboxylate or aqua ligands. On this basis, an average of <2 Å for the terminal ligand shell in the OEC would favor the presence of more O than N terminal ligands in the OEC. This is consistent with results from EPR and ESEEM experiments[9] that suggest a dominance of carboxylate-derived ligands on Mn in the protein.

Second Scatterer Shell. There is little controversy regarding the presence of Mn scatterers at 2.7 Å. The number of scatterers at 2.7 Å derived from curve-fitting falls between 1.0 and 1.5 per Mn in the OEC. These parameters are generally agreed upon by all investigators,[4,8b,c] with the exception of George et al.,[8a] who report 2.1 ± 0.8 scatterers at this distance. The reason for this disagreement is unclear at this time.

Third Scatterer Shell. The scatterers contributing to peak III are difficult to characterize due to the smaller amplitude of the peak and the possibility of more than one interaction at that distance. A common problem with the detection of metal scatterers at ~3 Å is the interference due to atoms from terminal ligands which, at the second bond position, fall at a distance of ~2.9–3.0 Å. In general, this problem in proteins has been addressed in EXAFS studies of the binuclear Fe systems of hemerythrin-like proteins and a number of associated binuclear model compounds.[20,26,29] The problem is compounded in EXAFS studies of the OEC in two ways: (1) The resolution in Mn EXAFS data in the OEC is limited by a smaller range of k. This is due to interfering X-ray fluorescence that occurs at $k \sim 12$ Å^{-1} from Fe in the OEC preparations. (2) The metal nuclearity is greater in the OEC and includes Mn–Mn distances at 2.7 Å as well as the longer distance. Here, we investigated the ability to analyze for longer Mn–Mn interactions in multinuclear systems using a set of Mn model compounds containing μ_2- or μ_3-oxo bridges, which result in Mn–Mn distances of >3 Å, in some cases in combination with Mn–Mn distances at 2.7 Å. For both the binuclear and trinuclear model complexes, the EXAFS analysis gave satisfactory results, with coordination numbers within 30% and distances within 0.04 Å of expected values. The tetranuclear complexes with several Mn–Mn interactions at ~3.3 Å were more difficult to model, with greater problems of disorder and interference from terminal ligands.

Qualitatively, the interactions at >3 Å in the OEC more closely resemble the EXAFS from the dimeric complex **1** in appearance and fitting characteristics (Figures 6 and 8; Tables 2 and 4). This favors a simple model for the OEC including just 1 Mn interaction at the >3-Å distance.

Possible combinations of Mn and Ca were tested in fitting the ≥3-Å interaction in the OEC. A Mn–Mn distance of >3 Å would be consistent with multinuclear models for the OEC, and Ca would be consistent with biochemical studies showing the influence of Ca on the EPR and activity of the OEC. The results from the fits presented here to the isolated peak III show a definite minimum fit error for fits including a heavy atom (Mn, Ca) over fits including only C atoms. In addition, the results for fits to the isolated peak III show a slightly lower fit error for combinations of atoms including Mn than for combinations including Ca. The average distances to these scatterers were found to be 3.3–3.4 Å. These results differ from those of MacLachlan et al.,[8c] who find a definite advantage in fitting their EXAFS to Ca, and at a longer distance of 3.7 Å. This distance is not consistent with our analysis (see Results). One possible reason for this disagreement could be in the methods of analysis: MacLachlan et al. hold the fit parameter

(29) (a) Scarrow, R. C.; Maroney, M. J.; Palmer, S. M.; Que, L., Jr.; Roe, A. L.; Salowe, S. P.; Stubbe, J. *J. Am. Chem. Soc.* **1987**, *109*, 7857–7864. (b) DeWitt, J. G.; Bentsen, J. G.; Rosenzweig, A. C.; Hedman, B.; Green, J.; Pilkington, S.; Papaefthymiou, G. C.; Dalton, H.; Hodgson, K. O.; Lippard, S. J. *J. Am. Chem. Soc.* **1991**, *113*, 9219–9235.

(30) Riggs, P. J.; Mei, R.; Yocum, C. F.; Penner-Hahn, J. E. *J. Am. Chem. Soc.* **1992**, *114*, 10650–10651.

ΔE to a single value while simultaneously refining all shells of scatterers, whereas we have found good agreement with Mn–scatterer distances in model compounds by leaving ΔE as a variable parameter for each shell. A second difference is in sample preparation. The samples reported here were prepared in buffers containing Ca^{2+}. In contrast, the samples for the other study were washed in buffers with no added Ca^{2+}. As they suggest,[8c] this difference in procedure may result in an altered environment of the Ca-binding site in their preparations.

Differences between S_1 and S_2 States. Results from X-ray absorption edge experiments[1c,4e,5] indicate that the advance of the OEC from the S_1 to the S_2 state is accompanied by the oxidation of a Mn(III) to a Mn(IV). A comparison of model compounds containing Mn(III) and Mn(IV) centers shows that the average bond lengths of terminal ligands to Mn(IV) are decreased by ~0.05–0.08 Å relative to those for Mn(III). In homologous bis(μ-oxo)-bridged binuclear complexes, oxidation from Mn^{III}–Mn^{IV} to Mn^{IV}_2 is accompanied by an increase in Mn–Mn distance of 0.01–0.05 Å.[6a] Such small changes diluted into a tetranuclear Mn complex may be very difficult to characterize in the EXAFS experiment. In this study, the small changes detected in the Fourier transforms of EXAFS of the OEC poised in S_1 and S_2 states are characterized by a lesser fit quality to the S_2 data, but the fit parameters do not show consistent differences. MacLachlan et al.[8c] find a slight increase in the terminal ligand distances upon advance from S_1 to S_2 in their samples. Interestingly, recent results from oriented EXAFS studies on layered PSII membranes indicate a slight *decrease* in Mn–terminal ligand distances upon advancing from the S_1 to the S_2 state.[31] Presumably, subsets of the terminal ligand set are sampled at different orientations, and analyses of these oriented data could give a better reflection of true ligand distances in the OEC.

Evaluation of Models for the OEC. The EXAFS data for the OEC in both PSII membranes from spinach and PSII particles from *Synechococcus* sp. contain scatterers at >3-Å average distance from the Mn and are dominated by contributions from short Mn–O interactions at 1.8 Å and Mn–Mn interactions at 2.7 Å. There are many possible ways to arrange four Mn atoms that include both Mn–Mn distances of both 2.7 and 3.3 Å. As previously noted,[4b–e,8] the results confirmed here of 2.0 ± 0.5 O at 1.8 Å and 1.2 ± 0.2 Mn at 2.7 Å per Mn are not consistent with the symmetric cubane to adamantane[32] or "butterfly" to distorted cubane[33] models that have been proposed for S-state transitions in the OEC. Several other types of possible structures are depicted in Figure 9. These are grouped roughly into "dimer of dimers" (**A**–**D**), "trimer–monomer" (**E**–**G**), and "tetranuclear" (**H**–**J**) clusters of four Mn. With the exception of **J**, these structures each contain a combination of ~2.7- and ~3.3-Å Mn–Mn vectors. Mn–Mn vectors of 2.7 Å are expected for structures bridged by two oxo species, and ~3.3-Å vectors are estimated for structures connected by a single oxo bridge. For convenience, both μ_2-oxo and μ_3-oxo bridges are approximated as having Mn–O distances of ~1.8 Å (all structures are assumed to contain Mn(III) or Mn(IV) and not Mn(II)), and carboxylato bridges are not included,

With the exception of **J**,[34] none of the structures in Figure 9 has yet been synthesized as a high-valent Mn compound. There are several similarities to existing inorganic models. A symmetric "dimer of dimers" model similar to **A** and **C** has been characterized, with a >4-Å distance between the bis(μ-oxo)-bridged binuclear

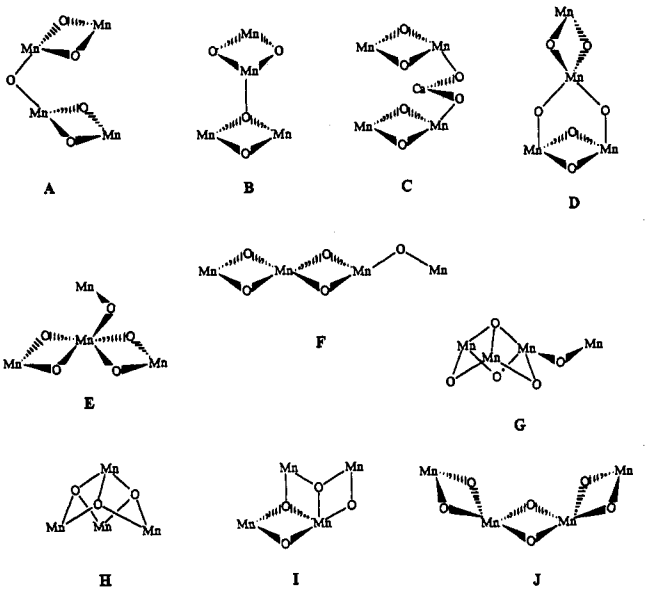

Figure 9. Arrangements of four Mn and associated bridging atoms giving Mn–Mn distances of 2.7 and >3 Å. The relations of these structures to existing tetranuclear Mn models is described in the text. The predicted coordination numbers for the neighboring Mn and bridging O atoms in these compounds are compared with those determined from EXAFS studies of the OEC in Table 5.

Table 5. Estimated Numbers of Scatterers for Selected Multinuclear Mn Structures

model	Mn–O (1.8 Å)	Mn–Mn (2.7 Å)	Mn–Mn, Ca (~3.3 Å)
OEC	1.5–2.5	1–1.5	0.5–1
A	2.5	1	0.5
B	2.25	1	1
C	2.5	1	1
D	3	1	1
E	2.5	1	0.5
F	2.5	1	0.5
G	2.75	1.5	0.5
H	2.25	1.5	1.5
I	2.5	1.5	1
J	3	1.5	

units.[6d,35] Model **E** is found as part of a higher nuclearity cluster,[36] and model **I** has been synthesized as $Mn^{II}_2Mn^{III}_2$.[37] The tetranuclear cluster **H** is closely approximated by the distorted Cl cubane described above.[28,33] Cluster **D** was recently pictured in a theoretical study,[38] and **C** was also recently proposed.[39]

For each of the structures shown in Figure 9, the expected numbers of scatterers (per Mn) for the bridge (O at ~1.8 Å), short metal (Mn at ~2.7 Å), and long metal (Mn at ~3.3 Å) interactions are listed in Table 5. Table 5 also includes the parameters for the OEC that are predicted from these EXAFS studies. The numbers of Mn–O scatterers in complexes **D** and **J** are somewhat higher than predicted from the OEC EXAFS. Protonation of a single bridge, however, could lengthen two Mn–O distances to the longer ≥1.9-Å distances included in the disordered terminal ligand shell for the OEC. The number of 1.5 Mn–Mn scatterers at 3.3 Å in complex **H**, the distorted cubane or pyramidal complex, is also higher than expected for the OEC. As discussed

(31) Mukerji, I.; Andrews, J.; DeRose, V. J.; Latimer, M. J.; Yachandra, V. K.; Sauer, K.; Klein, M. P. *Biochemistry*, submitted for publication.
(32) Brudvig, G. W.; Crabtree, R. H. *Proc. Natl. Acad. Sci. U.S.A.* **1986**, *83*, 4586–4588.
(33) Vincent, J. B.; Christou, G. *Inorg. Chim. Acta* **1987**, *136*, L41–L43.
(34) Philouze, C.; Blondin, G.; Ménage, S.; Auger, N.; Girerd, J.-J.; Vigner, D.; Lance, M.; Nierlich, M. *Angew. Chem., Int. Ed. Engl.* **1992**, *31*, 1629–1631.
(35) (a) Chan, M. K.; Armstrong, W. H. *J. Am. Chem. Soc.* **1991**, *113*, 5055–5057. (b) Kirk, M. L.; Chan, M. K.; Armstrong, W. H.; Solomon, E. I. *J. Am. Chem. Soc.* **1992**, *114*, 10432–10440.
(36) Low, D. W.; Eichhorn, D. M.; Draganescu, A.; Armstrong, W. H. *Inorg. Chem.* **1991**, *30*, 877–878.
(37) McKee, V.; Tandon, S. S. *J. Chem. Soc., Chem. Commun.* **1988**, 1334–1336.
(38) Proserpio, D. M.; Hoffmann, R.; Dismukes, G. C. *J. Am. Chem. Soc.* **1992**, *114*, 4374–4382.
(39) Philouze, C.; Blondin, G.; Girerd, J.-J.; Guilhem, J.; Pascard, C.; Klein, M. *J. Inorg. Biochem.* **1993**, *51*, 282.

above, the determination of numbers of scatterers at this distance in tetranuclear Mn complexes can be complicated. However, the longer-distance scatterers in the EXAFS of the OEC do resemble the scatterers in the simple "dimer" (1) both in a qualitative way and in fitting analysis behavior. This comparison favors single Mn–Mn scatterers at ~3.3 Å as found in complexes **A**, **E**, **F**, and **G**. Complex **A** is the simplest combination of distances and coordination numbers that fits the OEC EXAFS data and is also compatible with EPR[40] and orientation-dependent EXAFS studies on PSII membrane preparations.[31] For these reasons we have proposed it as a working model for the structure of the Mn complex in the OEC.[4c]

Acknowledgment. This work was supported by the National Science Foundation (Grant DMB91-04104), and by the Director, Division of Energy Biosciences, Office of Basic Energy Sciences, of the U.S. Department of Energy under contract DE-AC03-76SF00098. We thank Dr. Stephen Cramer for the use of his liquid-He cryostat and multielement Ge detector. We also thank Dr. Britton Chance for the use of his Ge detector. We are grateful to Dr. B. Hedman and Dr. S. Khalid for assistance at the beamlines and Dr. Jean-Luc Zimmermann for assistance in EXAFS data collection. We are deeply indebted to Professors W. H. Armstrong, G. Christou, J.-J. Girerd, and K. Wieghardt, and their respective research group members, for providing the multinuclear Mn model compounds used in these studies. Synchrotron radiation facilities were provided by the Stanford Synchrotron Radiation Laboratory (SSRL) and the National Synchrotron Light Source (NSLS), both supported by DOE. The Biotechnology Laboratory at SSRL and beamline X9-A at NSLS are supported by the National Center for Research Resources of the National Institutes of Health.

(40) Burghaus, O.; DeRose, V. J.; Liang, W.; Yachandra, V. K.; Klein, M. P. In *Research in Photosynthesis*; Murata, N., Ed.; Kluwer: Dordrecht, The Netherlands, 1992; Vol. II, pp 109–113.